Chinese Journal of Structural Chemistry 42 (2023) 100069

Contents lists available at ScienceDirect

Chinese Journal of Structural Chemistry

journal homepage: www.journals.elsevier.com/chinese-journal-of-structural-chemistry

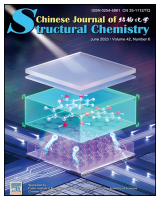

Article

Enhanced room temperature gas sensing performance of ZnO with atomic-level Pt catalysts facilitated by the polydopamine mediator

Qian Liu [a,b], Yingyi Wen [b], Jian-Ze Xiao [b], Shao-Zhen Luo [a,b], Guan-E Wang [b], Peng-Yi Tang [c], Xiao-Liang Ye [b,**], Gang Xu [b,*]

[a] College of Chemistry and Materials Science, Fujian Normal University, Fuzhou, 350007, China
[b] State Key Laboratory of Structural Chemistry, Fujian Institute of Research on the Structure of Matter, Chinese Academy of Sciences (CAS), Fuzhou, 350002, China
[c] Shanghai Institute of Microsystem and Information Technology, Chinese Academy of Science (CAS), Changning District, Shanghai, 200050, China

ARTICLE INFO

Keywords:
Atomic-level metal catalysts
ZnO nanorods
Polydopamine
Gas sensing
NO_2

ABSTRACT

The poor sensitivity of metal-oxide (MO) sensing material at room temperature can be enhanced by the modification of noble metal catalysts. However, the large size and uncontrollable morphology of metal nanoparticles (NPs) compromise the catalytic activity and selectivity. Downsizing metal NPs to the atomic level is a promising solution because it offers high activity and selectivity. Nevertheless, a facile and universal approach for stable loading atomic-level metal on MO-based sensing materials is still challenging. Herein, we present a strategy to construct synergetic coordination interface for uniform loading of atomic-level metal catalysts on MO-based gas-sensing materials using a difunctional mediator layer. In this work, atomically dispersed Pt catalysts are coordinately anchored on ZnO nanorods (NRs) using polydopamine (PDA) as a mediator. As a result, compared with pristine ZnO NRs, a six-fold enhanced response of 18,489% is achieved toward 100 ppm NO_2 on 0.20 wt% Pt–ZnO@PDA-1.5 nm, and the selectivity is also promoted. Such sensitivity is higher than that of most reported noble metal-modified MO NO_2-sensing materials. This work provides a simple and general strategy for building highly sensitive and selective gas-sensing materials using atomic-level noble metal catalyst.

1. Introduction

Gas-sensing technologies have attracted great attention in real-time air monitoring and healthcare [1–3]. The increased need for minimization and integration of gas sensors in smart systems requires the development of high-performance gas-sensing materials working at room temperature (RT) [4–8]. MO sensing materials have been widely researched and used for gas detection over the past several decades [9–13]. The gas-sensing performance of MOs usually relies on a high working temperature (100–400 °C), which is crucial for the generation of sufficient active oxygen species (O^{2-} and O^{-}) [14–16]. However, high working temperature degrades the stability of sensing materials while increasing device complexity and manufacturing cost [17,18]. The development of MO-based gas sensors with satisfactory sensitivity and selectivity at RT is important and challenging [15].

The atomic-level (single atom, dual atoms, and subnano-clusters) noble-metal catalysts with unsaturated coordination environment, unique electronic properties, and sufficient atomic utilization [19–22] can increase the sensitivity of MOs [20,21,23]. In addition, the selectivity of MO-based sensing material can be improved by atomic-level metal catalysts with highly uniform size and shape [24–26]. The reported strategies for dispersion of atomic-level metal catalysts on gas-sensing materials mainly focus on atomic layer deposition [27], pyrolysis [28], photochemical process [25], heteroatoms doping [29], sacrificial template [30], and defect engineering [31]. These strategies typically involve complicated procedures and high manufacturing cost and are limited to specific supporting materials. Therefore, a general, simple, and low-cost anchoring strategy for stable loading of atomic-level metal catalysts must be developed to achieve superior gas-sensing performance at RT.

An alternative method is to anchor atomic-level catalysts onto the surface of MO-based sensing materials through a mediator between them, which fundamentally offers diversity for the choice of metals and gas-sensing materials [32]. To achieve superior gas-sensing performance,

* Corresponding author.
** Corresponding author.
E-mail addresses: yexl@fjirsm.ac.cn (X.-L. Ye), gxu@fjirsm.ac.cn (G. Xu).

https://doi.org/10.1016/j.cjsc.2023.100069
Received 8 February 2023; Received in revised form 9 March 2023; Accepted 17 March 2023
Available online 21 March 2023

an ideal mediator should have large specific surface area, universal adhesivity, and abundant surface-anchoring sites. Such excellent mediator materials were rarely reported. The design and preparation of atomic-level metal catalysts loaded on MOs for gas-sensing remain challenging. PDA is a porous polymer with abundant catechol and amino groups, which can easily adhere to the surface of various materials to form a thin film with controllable thickness [33–35]. It provides a versatile platform for loading other species and facilitates the adsorption of gas molecules on the supporting material surface [36,37]. In addition, PDA can directly reduce various metal species to a lower valence state since they are anchored and dispersed by plentiful organic functional groups [38,39].

In this work, we report for the first time the construction of synergetic coordination interface using a difunctional mediator to anchor atomic-level catalysts on MO and improve RT gas-sensing performance. Dopamine molecules were self-assembled on the surface of ZnO NRs to form an ultra-thin PDA layer. The obtained ZnO@PDA-1.5 nm showed a response that is 2.6 times that of pristine ZnO toward NO_2 at RT under visible-light irradiation. Then, with the introduction of atomic-level Pt catalysts, 0.20 wt%Pt–ZnO@PDA-1.5 nm exhibited a six-fold improved response value compared with pristine ZnO under the same condition. Such sensitivity is higher than that of most reported noble metal-modified MO NO_2-sensing materials. The possible mechanism for the prominent sensitivity enhancement of Pt–ZnO@PDA-1.5 nm was revealed. We found that the ultra-thin PDA layer on ZnO NRs facilitated the adsorption of NO_2, and the anchored atomic-level Pt catalysts generated rich active oxygen species on ZnO owing to the high reactive activity and excellent spill-over effect of Pt. As a result, the synergetic effect of the PDA thin layer and atomic-level Pt catalysts enhanced the sensitivity of ZnO NRs to NO_2 at RT. This work offers a general approach for designing new high-performance gas-sensing materials, which are highly needed for environmental monitoring, healthcare, and the internet of things.

2. Results and discussion

2.1. Structural and morphological characterization of the samples

An ultrathin PDA layer was first grown on ZnO NRs (ZnO@PDA) by self-assembly of dopamine (details see experimental section). The core-shell structure was confirmed by TEM and energy dispersive spectroscopy (EDS) mapping. The thickness of PDA can be precisely controlled from 1 to 8 nm by adjusting the amount of added dopamine (Fig. 1a–e). In addition, N mapping in the EDS mapping covered the contour of Zn mapping, which suggested the successful coating of PDA layers on ZnO NRs (Fig. 1f).

After PDA coating, Pt was anchored onto ZnO@PDA NRs. The X-ray photoelectron spectroscopy (PXRD) pattern showed that the structures of ZnO NRs were maintained after PDA coating and Pt loading (Fig. 2a). No diffraction peaks of Pt NPs were found in the PXRD pattern of Pt-ZnO@PDA-1.5 nm, which indicated the low Pt contents and uniform dispersion of Pt species with ultra-small size. High-resolution TEM (HR-TEM) and high-angle annular dark-field scanning TEM (HAADF-STEM) were used to further confirm the atomical dispersion of Pt on 0.20 wt% Pt–ZnO@PDA-1.5 nm. As shown in Fig. S1, no Pt NPs were found in 0.20 wt%Pt–ZnO@PDA-1.5 nm. Meanwhile, EDS mapping (Fig. 2b) suggested that Pt was uniformly distributed throughout the ZnO NRs, revealing the successful loading of Pt catalysts. Furthermore, the AC-HAADF-STEM images (Figs. S2a and b) depicted that numerous single Pt atoms and several small clusters were uniformly dispersed, which suggest that Pt species were anchored at the atomic level onto ZnO NRs coated with PDA thin layer. By contrast, without the PDA mediating layer, Pt appeared as ununiformly distributed and unevenly sized NPs on ZnO nanorods as indicated by HR-TEM images (Figs. S2c and d). These results revealed that ZnO NRs with atomic-level Pt of controllable loading were successfully prepared via the assistance of the PDA thin layer.

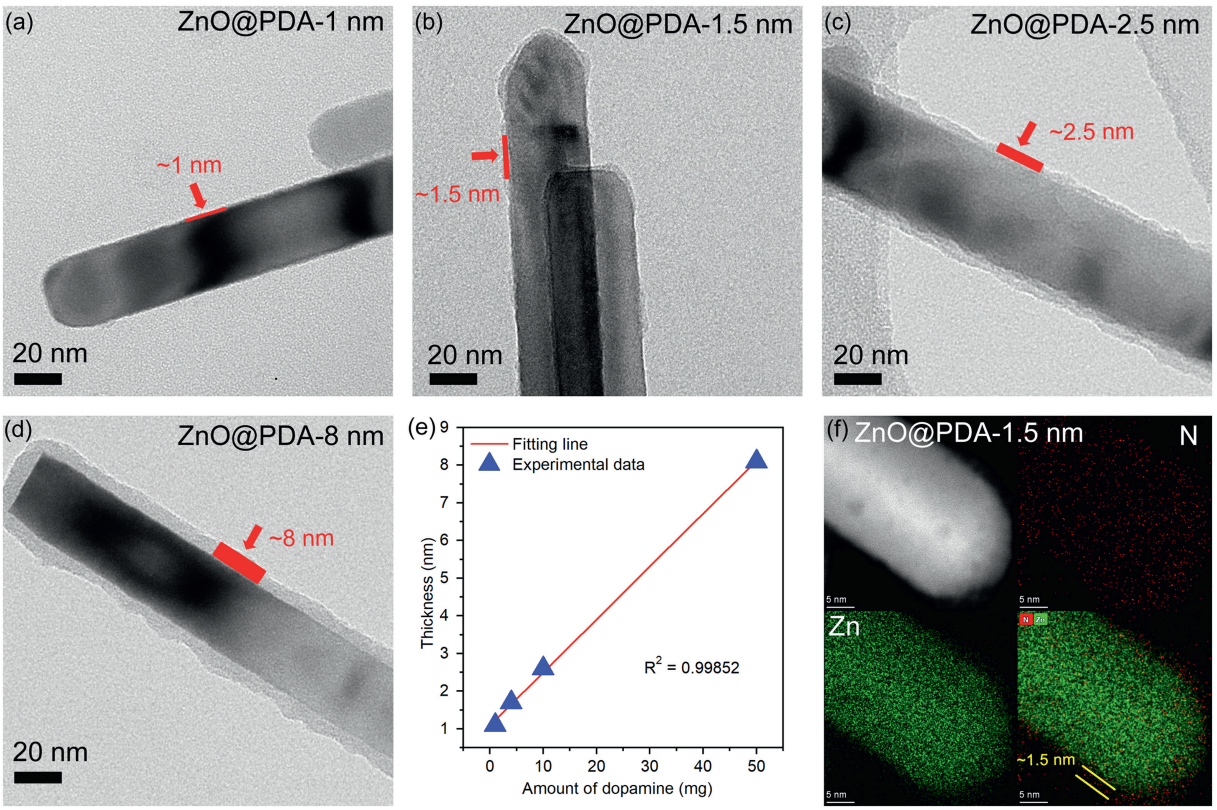

Fig. 1. (a–d) TEM images of ZnO@PDA with different PDA thicknesses. (c) Relationship of PDA thickness and dopamine added to the solution. (f) The STEM-EDS mapping images of ZnO@PDA-1.5 nm.

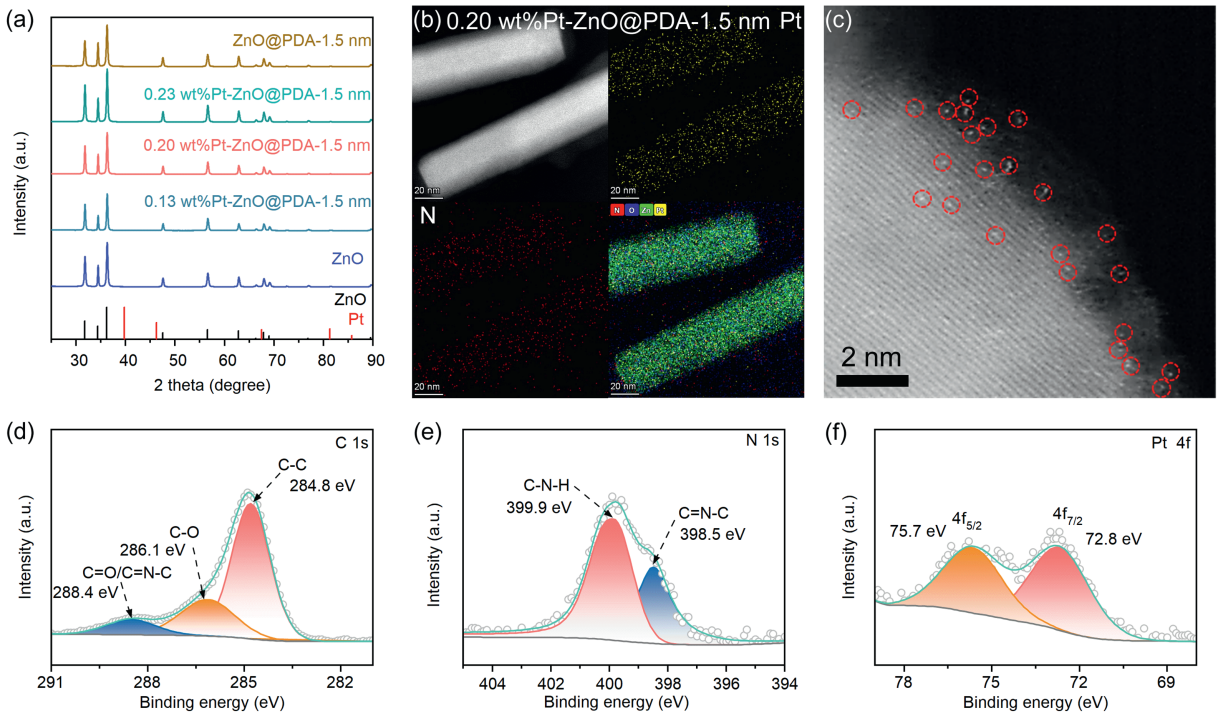

Fig. 2. (a) The PXRD patterns of all samples. (b) STEM-EDS mapping images of 0.20 wt%Pt–ZnO@PDA-1.5 nm. (c) AC-HAADF-STEM image of 0.20 wt% Pt–ZnO@PDA-1.5 nm. (d–f) XPS spectra of 0.20 wt%Pt–ZnO@PDA-1.5 nm. (d) C 1s spectrum, (e) N 1s spectrum and (f) Pt 4f spectrum.

X-ray photoelectron spectroscopy (XPS) was used to study the chemical composition of samples and the chemical state of elements. Notably, N 1s and Pt 4f peaks in the XPS survey spectra of 0.20 wt% Pt–ZnO@PDA-1.5 nm proved the presence of PDA mediator and Pt catalyst (Fig. S3). Typical binding energies for C 1s of C–C, C–O, and C=O/C=N–C bonds were found at 284.8, 286.1, and 288.4 eV, respectively (Fig. 2a) [40]. The N 1s spectrum (Fig. 2b) showed two fitted peaks at 398.5 and 399.9 eV, which were attributed to C=N–C and N–H of PDA coating, respectively [40]. The Pt 4f spectrum of XPS (Fig. 2c) was divided into two peaks, corresponding to Pt $4f_{5/2}$ and Pt $4f_{7/2}$ orbitals, respectively. The two fitted peaks (72.8 and 75.7 eV) indicated the valence of Pt is between +2 and +4, and closer to Pt(II) [26]. Such positive valence Pt should exhibit unique physical and chemical properties of atomic-level metals [19,22,32,41].

2.2. Gas sensing performance

To demonstrate the improvement of gas-sensing performance by coating PDA thin layer and introducing atomic-level Pt catalysts, the performance of pristine ZnO and ZnO@PDA control samples was also evaluated on our homemade test system [42]. PDA thickness and Pt loading were optimized to achieve the best overall performance. The ZnO@PDA-1.5 nm with 1.5 nm PDA thin-layer sensor showed the highest response toward NO_2 among the devices based on ZnO@PDA with different PDA layer thickness (Fig. 3a and S5b-e). Although the PDA powders showed no response to NO_2 (Figs. 3a and S5a), the PDA thin layer on ZnO@PDA-1.5 nm may facilitate the adsorption and accumulation of NO_2 molecules due to higher BET specific surface area than pristine ZnO, from 14.5 to 25.5 $m^2\ g^{-1}$ (Fig. S6). Different Pt metal feedings were then used to load different amounts of Pt on ZnO@PDA-1.5 nm, where 0.20 wt% (data acquired from the ICP-AES test) Pt loading delivered the highest response (Fig. S7). The 0.20 wt% Pt–ZnO@PDA-1.5 nm sensor exhibited much higher responses than the devices based on Pt NPs-ZnO. This demonstrated the unique advantage of atomic-level metal catalysts with the assistance of the PDA thin layer.

As shown in Fig. 3c, upon cyclic exposure to NO_2 with a concentration ranging from 1 to 100 ppm, the resistance of 0.20 wt%Pt–ZnO@PDA-1.5 nm sensors quickly exhibited prominent and reversible changes. Upon exposure to 100 ppm NO_2, the 0.20 wt%Pt–ZnO@PDA-1.5 nm sensor showed a response value of 18,489%, which was 6 and 2.6 times higher than that of the device based on pristine ZnO and ZnO@PDA-1.5 nm, respectively. The sensor also responded to NO_2 very quickly. The 0.20 wt% Pt–ZnO@PDA-1.5 nm sensor reached 90% of the response value after 22 s when exposed to 10 ppm NO_2 (Fig. 3d). By linear fitting the response-concentration relationship (Fig. 3e), a low limit of detection (LOD) of 108 ppb was extrapolated (the response threshold is set as 10%). Notably, the NO_2 sensitivity of 0.20 wt%Pt–ZnO@PDA-1.5 nm sensor surpassed that of most reported metal-modified MO gas sensors (Fig. 3e and Table S1). The selectivity of 0.20 wt%Pt–ZnO@PDA-1.5 nm sensor was evaluated by exposure to 13 typical interfering gaseous analytes with the same concentration of 100 ppm. 0.20 wt%Pt–ZnO@PDA-1.5 nm sensor showed considerably better selectivity than pristine ZnO. As shown in Figs. 3f and S6, 0.20 wt%Pt–ZnO@PDA-1.5 nm sensor exhibited negligible responses to interference analytes with high selectivity coefficient ($S = R_{NO2}/R_{other\ gas}$) ranging from 250 to 18,489. Cycling and long-term stability tests were also performed on 0.20 wt%Pt–ZnO@PDA-1.5 nm sensor. The devices showed an ultralow coefficient of variation (CV = 0.57%) after four successive exposures to 10 ppm NO_2, which suggests an excellent repeatability. As shown in Fig. S9, no evident sensitivity decay was observed for over 9 days, which indicates good stability of the material. To verify the interference of humidity, the response of 0.20 wt%Pt–ZnO@PDA-1.5 nm sensors to 10 ppm NO_2 was tested at different relative humidity (RH). The results (Fig. S10) show that the response value of 0.20 wt%Pt–ZnO@PDA-1.5 nm to 10 ppm NO_2 is 2043% at 10% RH, and the response value does not change significantly at different RH. The decrease in the response value at different RH may be due to the partial dissolution of NO_2 in water, which reduces the concentration of NO_2. Although the material showed a reduced response to NO_2 under humidity conditions, there was still a high response at different humidity levels, and NO_2 was detected under high humidity conditions.

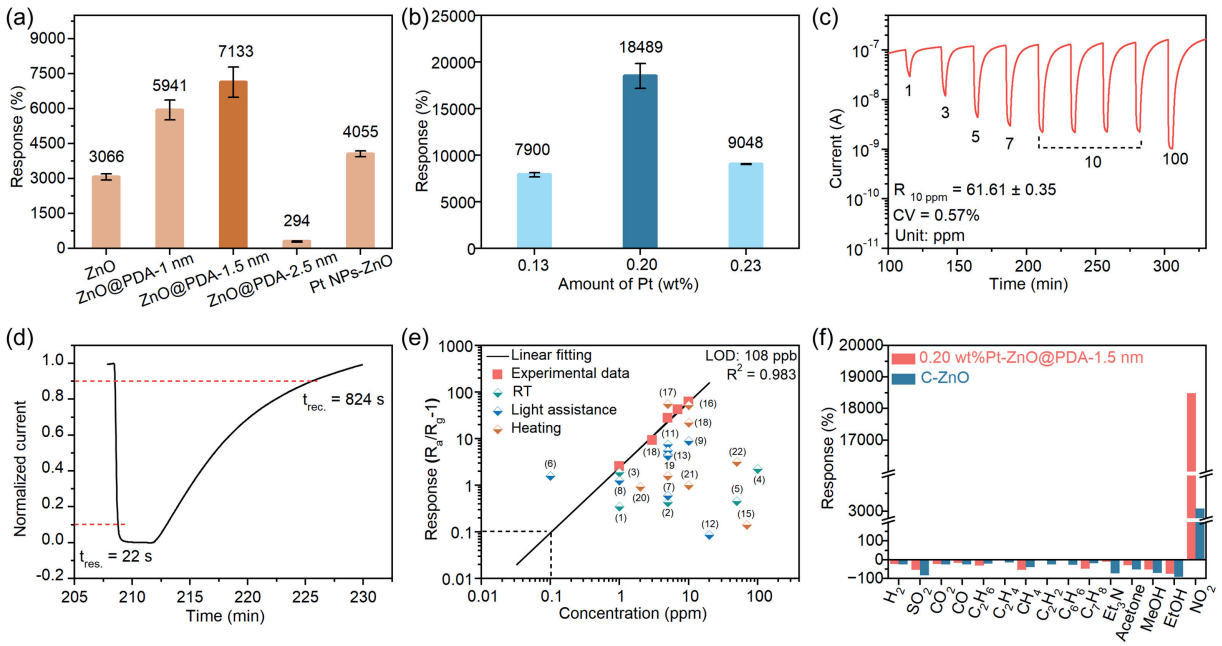

Fig. 3. Gas sensing performance of 0.20 wt%Pt–ZnO@PDA-1.5 nm and control samples at RT under visible light irradiation. (a) Responses of ZnO@PDA with different PDA thickness toward 100 ppm NO_2. (b) Responses of Pt–ZnO@PDA-1.5 nm with different Pt loading toward 100 ppm NO_2. (c) Typical response-recovery curve of the 0.20 wt%Pt–ZnO@PDA-1.5 nm sensor to NO_2 with different concentrations (1–100 ppm). (d) Response-recovery curves to 10 ppm NO_2. (e) Response concentration relationship of 0.20 wt%Pt–ZnO@PDA-1.5 nm to NO_2, and responses of representative NO_2 sensing materials based on noble metal nanoparticles modified metal oxide reported previously ((1) ZnO/SNO_2/Pt, (2) Pt–ZnO/PRGO, (3) Pt-decorated Bi_2O_3-branched SNO_2 NWs, (4) Au@Cu_2O core-shell NPs, (5) Pd/ZnO nanoparticles, (6) ZnO/Pd hybrids, (7) Au/ZnO films, (8) Au NPs/ZnO rods arrays, (9) Au nanoparticle-ZnO nanorods, (10) ZnO nanosheets/Au, (11) ZnO–Ag heterostructure nanoparticles, (12) WS_2/Au/ZnO nanorods, (13) Au–ZnO nanorod array thin films, (14) 0.1% Pt ZnO NWs Au nanoparticle-ZnO nanorods, (15) Pt NPs-ZnO, (16) Pt/ZnO/g-C_3N_4, (17) Hybrid ZnO@Au core-shell nanorods, (18) Pd-embedded SnO_2-x-decorated SnO_2 nanowires, (19) 1%-Ga-Pt@ZnO, (20) Pt Nanoparticles on ZnO-Branched SnO_2 Nanowires, (21) Au-functionalized CuO NWs, (22) Au/ZnO nanorods; see details in Table S1). (f) Response of 0.20 wt%Pt–ZnO@PDA-1.5 nm and ZnO sensor to different interfering gas with a concentration of 100 ppm.

2.3. Sensing mechanism

The sensing mechanism of 0.20 wt%Pt–ZnO@PDA-1.5 nm toward NO_2 can be primarily explained by the change in surface electron density, which was ascribed to the sensitive interaction between NO_2 and surface oxygen ion (O_2^-) of ZnO. The NO_2 adsorption test performed on MEMS cantilever chip demonstrated that the adsorption quantity of ZnO@PDA-1.5 nm (10.9 pg/ng) was higher than that of pristine ZnO (3.1 pg/ng) (Fig. S11). This result was attributed to the porous PDA film with rich catechol and amino groups, which increased the specific surface area and facilitated the adsorption and enrichment of NO_2 molecules on the ZnO surface. Under light irradiation with sufficient photon energy, electrons in the valence band of ZnO can be excited to the conduction band, which created photoelectron-hole pairs. Then, the photoinduced electrons reacted with the surrounding oxygen to form O_2^- ($h\nu$). O_2^- ($h\nu$) was weakly bound to ZnO and had a stronger reactivity than O_2^- (ads.), beneficial to RT gas sensing according to the reactions in Eqs. (1)–(3) [43]. Originally, the amount of O_2^- ($h\nu$) on pristine ZnO was insufficient for RT gas sensing. With the introduced high-activity Pt catalysts, more oxygen from the air can be absorbed to generate more O_2^- ($h\nu$).

$$h\nu \leftrightarrow h^+ + e^- \quad (1)$$

$$O_2\ (\text{ads.}) + e^- \leftrightarrow O_2^-\ (\text{ads.}) \quad (2)$$

$$O_2\ (\text{ads.}) + e^-\ (h\nu) \leftrightarrow O_2^-\ (h\nu) \quad (3)$$

To prove our speculation, we conducted XPS to reveal the change of O species before and after PDA thin-layer and Pt modification. The O 1s spectra of ZnO were deconvoluted to three peaks corresponding to lattice oxygen (O_L), adsorbed oxygen ion ($O_{ads.}$, that is, O_2^- in this work), and surface oxygen ($O_{surf.}$) which were located at 530.3, 530.7, and 531.9 eV, respectively (Fig. S12a) [44]. With the PDA thin-layer coating, ZnO@PDA-1.5 nm and 0.20 wt%Pt–ZnO@PDA-1.5 nm showed an extra peak corresponding to C–O (533.0 eV) (Figs. S12b and c) [45,46]. Notably, the result showed that the content ratio of $O_{ads.}/O_L$ was almost unchanged after PDA thin layer coating while it significantly increased from 0.66 to 1.81 after Pt loading (Fig. 4a). The atomic-level Pt catalysts with highly active sites can greatly promote the adsorption and dissociation of oxygen molecules, which can diffuse to the surface of ZnO through the spill-over effect and capture electrons from its conduction band to form O_2^- ($h\nu$) [14,47]. Given that abundant highly active Pt catalytic sites were introduced to the 0.20 wt%Pt–ZnO@PDA-1.5 nm sensor, the amount of O_2^- on the surface was largely increased. In addition, the atomic-level Pt can accelerate the transfer of electrons between molecules and the surface of ZnO, thus partially improving the sensor response [15]. In general, uniformly dispersive atomic-level Pt catalysts significantly enhanced the sensitivity of the ZnO-based gas sensor to NO_2.

To gain more insights into the interaction of sensing material and gas molecules, *in-situ* diffuse reflectance infrared Fourier transform spectroscopy (DRIFTS) was performed to monitor the sensing process of 0.20 wt%Pt–ZnO@PDA-1.5 nm when exposed to NO_2 (Fig. 4b). The time-resolved DRIFT spectra clearly showed the presence of adsorption peaks ascribed to NO_2 (1685 and 1634 cm^{-1}) and N_2O_4 (1779 cm^{-1}), whose intensity continuously increased upon extending the exposure time [48]. Meanwhile, other peaks attributed to monodentate nitrate (1322 cm^{-1}), bridging nitrate (1354 and 1031 cm^{-1}), and monodentate nitrite (1478 and 1053 cm^{-1}) were also observed [48–50]. We presume that in the interaction between NO_2 and 0.20 wt%Pt–ZnO@PDA-1.5 nm, NO_2 not only directly gained electrons from the conduction band of ZnO to form NO_2^- but also interacted with O_2^- ($h\nu$) and generated NO_3^-. According to

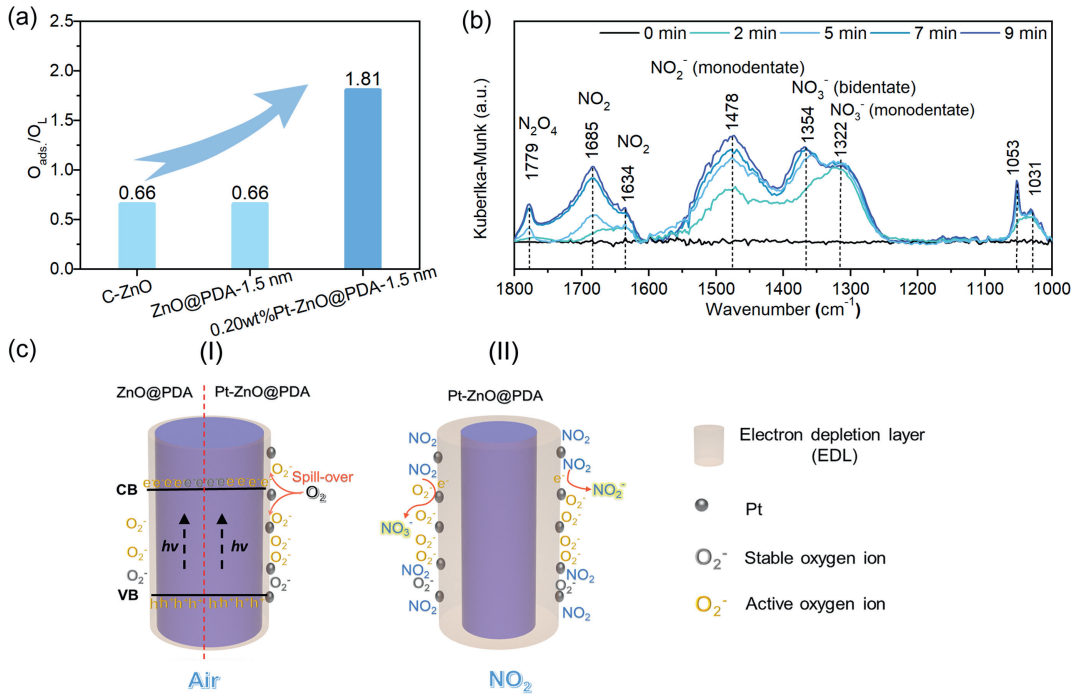

Fig. 4. (a) The propotion of $O_{ads.}/O_L$ calculated from O 1s spectra of C–ZnO, ZnO@PDA-1.5 nm, and 0.20 wt%Pt–ZnO@PDA-1.5 nm. (b) *In-situ* DRIFTS of 0.20 wt% Pt–ZnO@PDA-1.5 nm. (c) The proposed gas sensing mechanism of Pt–ZnO@PDA-1.5 nm toward NO_2 under visible light-activated and at RT.

the above results, the chemical process after injection of NO_2 can be represented by Eqs. (4)–(6).

$$2NO_2 \leftrightarrow N_2O_4 \tag{4}$$

$$NO_2 + e^- (h\nu) \leftrightarrow NO_2^- \tag{5}$$

$$2NO_2 + e^- (h\nu) + O_2^- (h\nu) \leftrightarrow 2NO_3^- \tag{6}$$

Based on the above evidence, we believe the sensitivity of Pt-ZnO@PDA-1.5 nm sensing material was enhanced by two main influencing factors: (1) PDA thin-layer coating on the ZnO surface which is beneficial to NO_2 adsorption and enrichment; (2) An increase in O_2^- ($h\nu$) due to the atomic-level Pt catalyst modification. As shown in Fig. 4c, the overall gas-sensing mechanism was proposed as follows. When Pt-ZnO@PDA-1.5 nm sensors were subjected to light irradiation in the air, the amount of O_2^- ($h\nu$) was increased after the modification of atomic-level Pt catalysts which have high reactive activity and spill-over effect (Fig. 4c (I)). When Pt–ZnO@PDA-1.5 nm sensor was exposed to NO_2, through synergistic coordination interface, a large number of NO_2 molecules were enriched by the PDA thin layer and reacted with sufficient active oxygen ions originating from atomic-level Pt catalysts and electrons. This process widened the electron depletion layer (EDL) of ZnO (Fig. 4c (II)) and caused the dramatic change in electron density which ultimately led to ultra-high sensing response.

3. Conclusion

In conclusion, to improve the RT gas-sensitive performance of MOs, we constructed synergetic coordination interface where a difunctional mediator was used to anchor an atomic-level catalyst onto MOs. Using *in-situ* polymerized PDA as a mediate coating, atomic-level Pt catalysts can be stably anchored and uniformly distributed on ZnO NRs. The Pt-loaded ZnO@PDA NRs showed an almost six-fold enhanced response of up to 18,489% to 100 ppm NO_2 compared with pristine ZnO NRs. A short response time of 22 s, an ultra-low LOD of 108 ppb and excellent selectivity were also realized. The superior performance was mainly ascribed to the synergetic effect of atomic-level Pt and PDA thin layer which offers sufficient highly active sites and enrichment of target molecules, respectively. This work may open a general way for the design of high-performance MOs-based gas-sensing materials at RT and inspire the application of atomic-level catalysts in gas-sensing.

4. Experimental

4.1. Materials

Chloroplatinic acid hexahydrate ($H_2PtCl_6{\cdot}6H_2O$), zinc acetate dihydrate ($Zn(CH_3COO)_2{\cdot}2H_2O$), and sodium hydroxide (NaOH) were purchased from Sigma-Aldrich. Dopamine hydrochloride and tris(hydroxy methyl)aminomethane (tris) were bought from Alfa Aesar (China). Urea was acquired from Aladdin Industrial Corporation. Ethanol was secured from Xinweicheng Co., Ltd. (Fuzhou, China). Unless otherwise noted, materials obtained from commercial suppliers were used without further purification. All aqueous solutions were prepared with Milli-Q water (18.2 MΩ). Ag–Pd interdigital electrode plates with a channel of 200 μm were obtained from Hangzhou Jinbo Tech. Co., Ltd., China.

4.2. Synthesis of ZnO NRs

ZnO NRs were prepared according to the reported literature with a modified synthetic method [51]. Briefly, $Zn(Ac)_2{\cdot}H_2O$ (0.22 g) and NaOH (0.4 g) were dissolved in 10 and 20 mL ethanol, respectively. Then, the above solutions were mixed, transferred to a Teflon-lined stainless-steel autoclave, and allowed to react at 150 °C for 24 h before the mixture was cooled to RT for 6 h. The mixture was then centrifuged and rinsed with water and ethanol thoroughly. After drying at 60 °C for 12 h, ZnO NRs were obtained and collected for characterization and further experiments.

4.3. Preparation of ZnO@PDA-thickness

ZnO@PDA-thickness NRs were prepared in accordance with a previous report using a modified synthesis method [52]. First, ZnO NRs were calcined at 200 °C in H_2 (5% in Ar) atmosphere for 1 h in a tube furnace

at a ramp rate of 2 °C min^{-1} and formed more oxygen vacancies. Then, 0.1 g calcined ZnO (C–ZnO) NRs was dispersed in 20 mL tris buffer solution (10 mM solution, pH 8.5) by ultrasonication. Then, *x* mg dopamine hydrochloride (*x* represents 1, 4, 10, and 50) was added to the ZnO suspension under stirring. The suspension was stirred for 6 h at RT. The products were washed with deionized water and ethanol for three times each and collected by centrifugation. After vacuum drying at 60 °C for 12 h, ZnO@PDA-thickness was obtained.

4.4. Preparation of Pt–ZnO@PDA-1.5 nm

A total of 6, 10, and 16 mg urea were dissolved in 50 mL deionized water. Then, the as-prepared ZnO@PDA-1.5 nm was added to the solution and ultrasonicated for 30 min. Subsequently, *y* μL (*y* is 15, 25, and 40) of H_2PtCl_6 aqueous solution (25 mg mL^{-1}) was added and stirred for 3 h at RT. The mixture was then centrifuged and rinsed with deionized water and ethanol three times. After drying at 60 °C for 12 h, Pt-ZnO@PDA-1.5 nm with different amounts of Pt was obtained.

Pt NPs-ZnO was prepared by a simple method. A total of 0.1 g C–ZnO NRs were dispersed in 150 mL deionized water. Then, 200 mL H_2PtCl_6 aqueous solution (25 mg mL^{-1}) was added. Subsequently, 20 mL sodium borohydride in methanol (2.5 mg mL^{-1}) was added, and the mixture was stirred for 2 h at 60 °C. The mixture was then centrifuged and rinsed with deionized water and ethanol for three times each.

4.5. Characterization

Morphological details were examined using transmission electron microscopy (TEM, Tecnai F20). HAADF-STEM images were collected on a JEOL JEM-2100F. The nitrogen adsorption/desorption measurement was performed using a Micromeritics ASAP2020 gas-sorption system. PXRD was conducted on a Rigaku Smartlab X-ray diffractometer with Cu Kα radiation (λ = 1.5406 Å) at a scanning speed of 10 ° min^{-1}. Aberration-corrected HAADF-STEM (AC-HAADF-STEM) images were collected on STEM equipment with a CEOS probe corrector. The data of XPS were collected on a thermos scientific ESCALAN 250 Xi XPS system (monochromatic Al Kα X-rays (1486.6 eV) operating at 15 kV; base pressure: 5.0×10^{-8} Pa). Weight percentage of loaded noble metal was measured using inductively coupled plasma atomic emission spectrometer (ICP-AES). The gas adsorption was measured by the MEMS cantilever (LoC-TGA 3000) chips connecting the computer to collect frequency signals and Molecular Adsorption Analyzer purchased from High-End MEMS Technology Co., Ltd. The *in-situ* DRIFTS experiments were performed on a Nicolet 6700 Fourier transform IR spectrometer equipped with stainless-steel *in-situ* IR flow cell and set up for diffuse reflectance sampling.

4.6. Gas sensing measurement

Gas sensors were fabricated by a drop-casting method. The prepared samples were dispersed in isopropanol. Subsequently, the dispersion containing an appropriate amount of sample was drop-casted on the Ag–Pd interdigital electrode. As shown in Fig. S4, the sensor testing performance was evaluated by a homemade system reported in our early work [42]. The flow for injection of synthetic air and analyte gas was 600 mL min^{-1}. A constant bias of 5 V was applied to the sensor, and the current was measured using a Keithley 2602B source meter. Gases with different concentrations were generated by mixing the standard analyte gas with synthetic air at different ratios. The gas-sensing performance of all samples toward poisonous NO_2 was evaluated at RT with the assistance of visible light (450 nm). The sensor was placed in a quartz tube with a flat window for light irradiation. A xenon lamp was mounted at 5 cm, and light was shed directly onto the sensor surface. The sensor response was defined as $(|R_g - R_a|/R_a) \times 100\%$ or $|R_g - R_a|/R_a$, where R_a and R_g are the device resistance under synthetic air and during exposure to analyte gases, respectively. The response/recovery time was defined as the time required to reach 90% resistance changes in the response/recovery curves, respectively.

Declaration of competing interest

The authors declare no competing interests.

Acknowledgements

This work was supported by the National Natural Science Foundation of China (91961115, 22171263, 21975254, and 22271281), Scientific Research and Equipment Development Project of CAS (YJKYQ20210024), Fujian Science & Technology Innovation Laboratory for Optoelectronic Information of China (2021ZR101), the Natural Science Foundation of Fujian Province (2021J02017, 2022J05088 and 2022J06032), and CAS Pioneer Hundred Talents Program B (E2XBRD1).

Appendix A. Supplementary data

Supplementary data to this article can be found online at https://doi.org/10.1016/j.cjsc.2023.100069.

References

[1] E. Gonzalez, C.J. Casanova, A. Romero, X. Vilanova, J. Mitrovics, E. Llobet, LoRa sensor network development for air quality monitoring or detecting gas leakage events, Sensors 20 (2020) 6225, https://doi.org/10.3390/s20216225.
[2] N. Alexis, C. Barnes, I.L. Bernstein, J.A. Bernstein, A. Nel, D. Peden, D. Diaz-Sanchez, S.M. Tarlo, P.B. Williams, Health effects of air pollution, J. Allergy Clin. Immunol. 114 (2004) 1116–1123, https://doi.org/10.1016/j.jaci.2004.08.030.
[3] R. Kumar, D.O. Al, G. Kumar, A. Umar, Zinc oxide nanostructures for NO_2 gas-sensor applications: a review, Nano-Micro Lett. 7 (2015) 97–120, https://doi.org/10.1007/s40820-014-0023-3.
[4] N. Joshi, T. Hayasaka, Y. Liu, H. Liu, O.N. Oliveira, L. Lin, A review on chemiresistive room temperature gas sensors based on metal oxide nanostructures, graphene and 2D transition metal dichalcogenides, Mikrochim. Acta 185 (2018) 213, https://doi.org/10.1007/s00604-018-2750-5.
[5] P. Srinivasan, M. Ezhilan, A.J. Kulandaisamy, K.J. Babu, J.B.B. Rayappan, Room temperature chemiresistive gas sensors: challenges and strategies—a mini review, J. Mater. Sci. Mater. Electron. 30 (2019) 15825–15847, https://doi.org/10.1007/s10854-019-02025-1.
[6] J. Zhang, X. Liu, G. Neri, N. Pinna, Nanostructured materials for room-temperature gas sensors, Adv. Mater. 28 (2016) 795–831, https://doi.org/10.1002/adma.201503825.
[7] L.X. Ou, M.Y. Liu, L.Y. Zhu, D.W. Zhang, H.L. Lu, Recent progress on flexible room-temperature gas sensors based on metal oxide semiconductor, Nano-Micro Lett. 14 (2022) 206, https://doi.org/10.1007/s40820-022-00956-9.
[8] Y. Jian, W. Hu, Z. Zhao, P. Cheng, H. Haick, M. Yao, W. Wu, Gas sensors based on chemi-resistive hybrid functional nanomaterials, Nano-Micro Lett. 12 (2020) 71, https://doi.org/10.1007/s40820-020-0407-5.
[9] H. Ji, W. Zeng, Y. Li, Gas sensing mechanisms of metal oxide semiconductors: a focus review, Nanoscale 11 (2019) 22664–22684, https://doi.org/10.1039/c9nr07699a.
[10] J. Zhang, Z. Qin, D. Zeng, C. Xie, Metal-oxide-semiconductor based gas sensors: screening, preparation, and integration, Phys. Chem. Chem. Phys. 19 (2017) 6313–6329, https://doi.org/10.1039/c6cp07799d.
[11] T. Lin, X. Lv, Z. Hu, A. Xu, C. Feng, Semiconductor metal oxides as chemoresistive sensors for detecting volatile organic compounds, Sensors 19 (2019) 233, https://doi.org/10.3390/s19020233.
[12] A. Mirzaei, H.W. Kim, S.S. Kim, G. Neri, Nanostructured semiconducting metal oxide gas sensors for acetaldehyde detection, Chemosensors 7 (2019) 56, https://doi.org/10.3390/chemosensors7040056.
[13] R. Kumar, X. Liu, J. Zhang, M. Kumar, Room-temperature gas sensors under photoactivation: from metal oxides to 2D materials, Nano-Micro Lett. 12 (2020) 164, https://doi.org/10.1007/s40820-020-00503-4.
[14] L. Zhu, W. Zeng, Room-temperature gas sensing of ZnO-based gas sensor: a review, Sensor Actuat. A Phys. 267 (2017) 242–261, https://doi.org/10.1016/j.sna.2017.10.021.
[15] Z. Li, H. Li, Z. Wu, M. Wang, J. Luo, H. Torun, P. Hu, C. Yang, M. Grundmann, X. Liu, Y. Fu, Advances in designs and mechanisms of semiconducting metal oxide nanostructures for high-precision gas sensors operated at room temperature, Mater. Horiz. 6 (2019) 470–506, https://doi.org/10.1039/c8mh01365a.
[16] Z. Li, Y. Huang, S. Zhang, W. Chen, Z. Kuang, D. Ao, W. Liu, Y. Fu, A fast response & recovery H_2S gas sensor based on α-Fe_2O_3 nanoparticles with ppb level detection limit, J. Hazard Mater. 300 (2015) 167–174, https://doi.org/10.1016/j.jhazmat.2015.07.003.
[17] C. Wang, L. Yin, L. Zhang, D. Xiang, R. Gao, Metal oxide gas sensors: sensitivity and influencing factors, Sensors 10 (2010) 2088–2106, https://doi.org/10.3390/s100302088.

[18] T. Gessner, K. Gottfried, R. Hoffmann, C. Kaufmann, U. Weiss, E. Charetdinov, P. Hauptmann, R. Lucklum, B. Zimmermann, U. Dietel, G. Springer, M. Vogel, Metal oxide gas sensor for high temperature application, Microsyst. Technol. 6 (2000) 169–174, https://doi.org/10.1007/s005420000048.
[19] C.C. Hou, H.F. Wang, C. Li, Q. Xu, From metal-organic frameworks to single/dual-atom and cluster metal catalysts for energy applications, Energy Environ. Sci. 13 (2020) 1658–1693, https://doi.org/10.1039/c9ee04040d.
[20] Y. Fan, S. Liu, Y. Yi, H. Rong, J. Zhang, Catalytic nanomaterials toward atomic levels for biomedical applications: from metal clusters to single-atom catalysts, ACS Nano 15 (2021) 2005–2037, https://doi.org/10.1021/acsnano.0c06962.
[21] T. Chao, Y. Hu, X. Hong, Y. Li, Design of noble metal electrocatalysts on an atomic level, ChemElectroChem 6 (2019) 289–303, https://doi.org/10.1002/celc.201801189.
[22] X.F. Yang, A. Wang, B. Qiao, J. Li, J. Liu, T. Zhang, Single-atom catalysts: a new frontier in heterogeneous catalysis, Acc. Chem. Res. 46 (2013) 1740–1748, https://doi.org/10.1021/ar300361m.
[23] B. Liu, L. Zhang, Y. Luo, L. Gao, G. Duan, The dehydrogenation of H–S bond into sulfur species on supported Pd single atoms allows highly selective and sensitive hydrogen sulfide detection, Small 17 (2021) 2105643, https://doi.org/10.1002/smll.202105643.
[24] G. Lei, H. Pan, H. Mei, X. Liu, G. Lu, C. Lou, Z. Li, J. Zhang, Emerging single atom catalysts in gas sensors, Chem. Soc. Rev. 51 (2022) 7260–7280, https://doi.org/10.1039/d2cs00257d.
[25] X.L. Ye, S.J. Lin, J.W. Zhang, H.J. Jiang, L.A. Cao, Y.Y. Wen, M.S. Yao, W.H. Li, G.E. Wang, G. Xu, Boosting room temperature sensing performances by atomically dispersed Pd stabilized via surface coordination, ACS Sensors 6 (2021) 1103–1110, https://doi.org/10.1021/acssensors.0c02369.
[26] H. Shin, W.-G. Jung, D.-H. Kim, J.-S. Jang, Y.H. Kim, W.-T. Koo, J. Bae, C. Park, S.-H. Cho, B.J. Kim, I.D. Kim, Single-atom Pt stabilized on one-dimensional nanostructure support via carbon nitride/SnO_2 heterojunction trapping, ACS Nano 14 (2020) 11394–11405, https://doi.org/10.1021/acsnano.0c03687.
[27] Y. Xu, W. Zheng, X. Liu, L. Zhang, L. Zheng, C. Yang, N. Pinna, J. Zhang, Platinum single atoms on tin oxide ultrathin films for extremely sensitive gas detection, Mater. Horiz. 7 (2020) 1519–1527, https://doi.org/10.1039/d0mh00495b.
[28] J. Qiu, X. Hu, L. Shi, J. Fan, X. Min, W. Zhang, J. Wang, Enabling selective, room-temperature gas detection using atomically dispersed Zn, Sensor. Actuat. B, Chem. 329 (2021) 129221, https://doi.org/10.1016/j.snb.2020.129221.
[29] Z. Xue, M. Yan, X. Wang, Z. Wang, Y. Zhang, Y. Li, W. Xu, Y. Tong, X. Han, C. Xiong, W. Wang, M. Chen, B. Ye, X. Hong, L. Song, H. Zhang, L.-M. Yang, Y. Wu, Tailoring unsymmetrical-coordinated atomic site in oxide-supported Pt catalysts for enhanced surface activity and stability, Small 17 (2021) 2101008, https://doi.org/10.1002/smll.202101008.
[30] H. Shin, J. Ko, C. Park, D.H. Kim, J. Ahn, J.S. Jang, Y.H. Kim, S.H. Cho, H. Baik, I.D. Kim, Sacrificial template-assisted synthesis of inorganic nanosheets with high-loading single-atom catalysts: a general approach, Adv. Funct. Mater. 32 (2021) 2110485, https://doi.org/10.1002/adfm.202110485.
[31] F. Gu, M. Di, D. Han, S. Hong, Z. Wang, Atomically dispersed Au on In_2O_3 nanosheets for highly sensitive and selective detection of formaldehyde, ACS Sensors 5 (2020) 2611–2619, https://doi.org/10.1021/acssensors.0c01074.
[32] C. Gao, J. Low, R. Long, T. Kong, J. Zhu, Y. Xiong, Heterogeneous single-atom photocatalysts: fundamentals and applications, Chem. Rev. 120 (2020) 12175–12216, https://doi.org/10.1021/acs.chemrev.9b00840.
[33] F. Bernsmann, V. Ball, F. Addiego, A. Ponche, M. Michel, J.J. Gracio, V. Toniazzo, D. Ruch, Dopamine-melanin film deposition depends on the used oxidant and buffer solution, Langmuir 27 (2011) 2819–2825, https://doi.org/10.1021/la104981s.
[34] K. Qu, Y. Zheng, S. Dai, S.Z. Qiao, Polydopamine-graphene oxide derived mesoporous carbon nanosheets for enhanced oxygen reduction, Nanoscale 7 (2015) 12598–12605, https://doi.org/10.1039/c5nr03089g.
[35] H. Lee, S.M. Dellatore, W.M. Miller, P.B. Messersmith, Mussel-inspired surface chemistry for multifunctional coatings, Science 318 (2007) 426–430, https://doi.org/10.1126/science.1147241.
[36] Z. Kang, D. Zhang, T. Li, X. Liu, X. Song, Polydopamine-modified SnO_2 nanofiber composite coated QCM gas sensor for high-performance formaldehyde sensing, Sensor. Actuat. B, Chem. 345 (2021) 130299, https://doi.org/10.1016/j.snb.2021.130299.
[37] D. Yan, P. Xu, Q. Xiang, H. Mou, J. Xu, W. Wen, X. Li, Y. Zhang, Polydopamine nanotubes: bio-inspired synthesis, formaldehyde sensing properties and thermodynamic investigation, J. Mater. Chem. 4 (2016) 3487–3493, https://doi.org/10.1039/c6ta00396f.
[38] M. Zhang, Y.G. Wang, W. Chen, J. Dong, L. Zheng, J. Luo, J. Wan, S. Tian, W.C. Cheong, D. Wang, Y. Li, Metal (hydr)oxides@polymer core-shell strategy to metal single-atom materials, J. Am. Chem. Soc. 139 (2017) 10976–10979, https://doi.org/10.1021/jacs.7b05372.
[39] L. Yan, X. Bo, D. Zhu, L. Guo, Well-dispersed Pt nanoparticles on polydopamine-coated ordered mesoporous carbons and their electrocatalytic application, Talanta 120 (2014) 304–311, https://doi.org/10.1016/j.talanta.2013.12.031.
[40] W. Ye, Y. Chen, Y. Zhou, J. Fu, W. Wu, D. Gao, F. Zhou, C. Wang, D. Xue, Enhancing the catalytic activity of flowerike Pt nanocrystals using polydopamine functionalized graphene supports for methanol electrooxidation, Electrochim. Acta 142 (2014) 18–24, https://doi.org/10.1016/j.electacta.2014.06.161.
[41] M. Hubner, D. Koziej, J.D. Grunwaldt, U. Weimar, N. Barsan, An Au clusters related spill-over sensitization mechanism in SnO_2-based gas sensors identified by operando HERFD-XAS, work function changes, DC resistance and catalytic conversion studies, Phys. Chem. Chem. Phys. 14 (2012) 13249–13254, https://doi.org/10.1039/c2cp41349c.
[42] M.S. Yao, W.X. Tang, G.E. Wang, B. Nath, G. Xu, MOF thin film-coated metal oxide nanowire array: significantly improved chemiresistor sensor performance, Adv. Mater. 28 (2016) 5229–5234, https://doi.org/10.1002/adma.201506457.
[43] S.W. Fan, A.K. Srivastava, V.P. Dravid, UV-activated room-temperature gas sensing mechanism of polycrystalline ZnO, Appl. Phys. Lett. 95 (2009) 142106, https://doi.org/10.1063/1.3243458.
[44] Z. Li, C. Lou, G. Lei, G. Lu, H. Pan, X. Liu, J. Zhang, Regulation of electronic properties of ZnO/In_2O_3 heterospheres via atomic layer deposition for high performance NO_2 detection, CrystEngComm 23 (2021) 5060–5069, https://doi.org/10.1039/d1ce00643f.
[45] Y. Ding, L.T. Weng, M. Yang, Z. Yang, X. Lu, N. Huang, Y. Leng, Insights into the aggregation/deposition and structure of a polydopamine film, Langmuir 30 (2014) 12258–12269, https://doi.org/10.1021/la5026608.
[46] N. Nie, F. He, L. Zhang, B. Cheng, Direct Z-scheme PDA-modified ZnO hierarchical microspheres with enhanced photocatalytic CO_2 reduction performance, Appl. Surf. Sci. 457 (2018) 1096–1102, https://doi.org/10.1016/j.apsusc.2018.07.002.
[47] D.W. Kim, K.H. Park, S.H. Lee, C. Fabrega, J.D. Prades, J.W. Jang, Plasmon expedited response time and enhanced response in gold nanoparticles-decorated zinc oxide nanowire-based nitrogen dioxide gas sensor at room temperature, J. Colloid Interface Sci. 582 (2021) 658–668, https://doi.org/10.1016/j.jcis.2020.08.082.
[48] M. Chen, Z. Wang, D. Han, F. Gu, G. Guo, High-sensitivity NO_2 gas sensors based on flower-like and tube-like ZnO nanomaterials, Sensor. Actuat. B, Chem. 157 (2011) 565–574, https://doi.org/10.1016/j.snb.2011.05.023.
[49] M. Chen, Z. Wang, D. Han, F. Gu, G. Guo, Porous ZnO polygonal nanoflakes: synthesis, use in high-sensitivity NO_2 gas sensor, and proposed mechanism of gas sensing, J. Phys. Chem. C 115 (2011) 12763–12773, https://doi.org/10.1021/jp201816d.
[50] L. Yang, A. Marikutsa, M. Rumyantseva, E. Konstantinova, N. Khmelevsky, A. Gaskov, Quasi similar routes of NO_2 and NO sensing by nanocrystalline WO_3: evidence by in situ DRIFT spectroscopy, Sensors 19 (2019) 3405, https://doi.org/10.3390/s19153405.
[51] B. Cheng, E.T. Samulski, Hydrothermal synthesis of one-dimensional ZnO nanostructures with different aspect ratios, Chem (2004) 986–987, https://doi.org/10.1039/b316435g.
[52] A. Han, J. Zhang, W. Sun, W. Chen, S. Zhang, Y. Han, Q. Feng, L. Zheng, L. Gu, C. Chen, Q. Peng, D. Wang, Y. Li, Isolating contiguous Pt atoms and forming Pt–Zn intermetallic nanoparticles to regulate selectivity in 4-nitrophenylacetylene hydrogenation, Nat. Commun. 10 (2019) 3787, https://doi.org/10.1038/s41467-019-11794-6.